COBEM 2023 27TH INTERNATIONAL CONGRESS OF MECHANICAL ENGENEERING

ABCM Brazilian Society of Mechanical Sciences and Engineering
27th ABCM International Congress of Mechanical Engineering
December 04-08, 2023, Florianópolis-SC, Brazil

COB-2023-2275
STABILITY ANALYSIS OF BOUNDARY LAYER FLOW IN HIGH ASPECT RATIO GAP UNDER BYPASS TRANSITION CONDITIONS.

Henrique Dias Teixeira
Marcello Augusto Faraco de Medeiros
Victor Barcelos Victorino
Felipe Oliveira Aguirre
USP - Av. Trab. São Carlense, 400 - Parque Arnold Schimidt, São Carlos - SP, 13566-590
henriquedt@usp.br
marcello@sc.usp.br
barcelos.victorino@usp.br
felipe.aguirre@usp.br

Abstract. *Boundary layer transition significantly affects aerodynamic drag. Accurately predicting the transition location requires understanding the boundary layer's stability, especially as real aircraft boundary layers often contain surface imperfections such as gaps. This study aims to investigate the influence of high aspect ratio gaps on boundary layer stability near bypass transition conditions reported in the literature. We used a numerical approach via two-dimensional direct numerical simulation to obtain the equilibrium solution of the compressible Navier-Stokes Equations, followed by a stability analysis of the flow to two- and three-dimensional disturbances. Our in-house algorithm, which uses an Arnoldi-based time-stepping method, was employed for linear stability analysis. Our preliminary results revealed unstable oscillation modes for 2D (Rossiter) analysis in the runs immediately following the bypass transition, suggesting a potential relationship between the Rossiter mode and the bypass transition reported in the literature.*

Keywords: *Boundary Layer, Navier-Stokes Equations, Rossiter modes, Open cavity*

1. INTRODUCTION

Aircraft performance is largely related to lift and drag ratio. Concerning drag, some of the reasons for its increase are imperfections or discontinuities in the aerodynamic body, whether intentional or not. They can be purposeful, such as slats and flaps, which generate discontinuities in aerodynamics surfaces. However, there are also unwanted imperfections, such as small spaces between plating that make up the aircraft wing. These spacings generate a significant impact on the boundary layer because once the flow interacts with it, the boundary layer can be disturbed. When disturbed, the boundary layer can have the transition location to turbulence altered, and if this occurs upstream than usual, due to these cavities, the drag increment is enhanced. The boundary layer transition phenomenon is naturally caused by Tollmien-Schlichting (T-S) mode.Figure 1 from Crouch *et al.* (2022) exhibits the impact on the transition position as a function of the geometry of the cavities. Note that the cavity dimensions are normalized by δ^*, the boundary layer displacement thickness at the gap. Markers in black indicate that the transition has shifted upstream. The red-filled dots indicate that the cavity has a large influence on the transition location. Furthermore, the authors measured a frequency quite different from that expected by a T-S, indicating a bypass transition. Beguet *et al.* (2017) also found bypass transition and the limits measured by them agreed with the results from Crouch *et al.* (2022), as indicated by the blue dashed lines in Fig. 1.

The literature presents cavity-related instabilities, such as instability Rossiter (1964) and centrifugal modes. Regarding the Rossiter instability, it occurs due to a feedback mechanism between vortex emission and acoustic waves produced by the shock of the vortices at the trailing edge of the cavity. Recent developments in the comprehension of this mode are presented in Rowley *et al.* (2002), Yamouni *et al.* (2013), Sun *et al.* (2017), and Mathias and Medeiros (2021). Concerning the centrifugal instability, Brès and Colonius (2008), de Vicente *et al.* (2014), and Meseguer-Garrido *et al.* (2014) provides a rich study on its characteristics. The numerical study from Brès and Colonius (2008) found three centrifugal modes, modes I, II, and III, classified according to their temporal frequency, which is considerably lower than the typical frequency of the Rossiter mode. The mode I is a stationary mode, and mode III presents a relatively low frequency. Unstable modes appeared with a spanwise wavelength normalized by the cavity depth λ/D within the range of $0.5 \geq \lambda/D \geq 1.5$. The authors point out that centrifugal instability occurs due to a decrease in the momentum caused by the cavity walls' presence. As a consequence, the angular velocity decreases in the radial direction, as it moves away from the vortex core inside the cavity. Because of this, the fluid is redirected towards the cavity spanwise, forming cellular patterns. Meseguer-Garrido *et al.* (2014) also characterized the centrifugal instability for different spanwise wavenumber, cavity dimensions, and Reynolds numbers. The authors also found two different modes, including the stationary mode

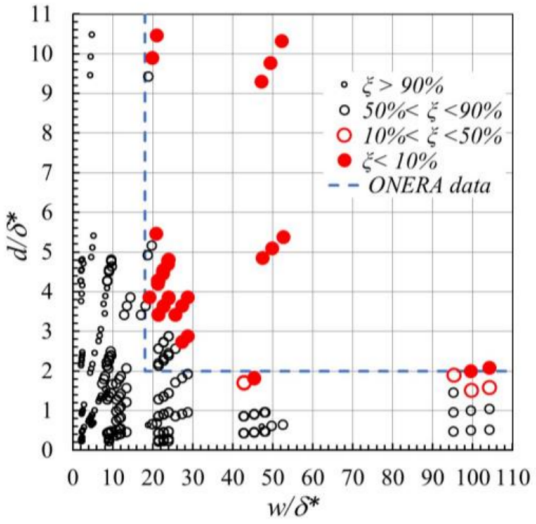

Figure 1. Diagram of the influence of the gap dimensions on the transition, taken from Crouch *et al.* (2022).

(null temporal frequency), which is the outcome of the bifurcation of a pair of conjugated complex modes that collapses into two stationary modes, one stable and the other unstable. This occurred for a relatively large value of β.

Considering that those are different instability modes than the natural instability observed in flat plates, the T-S mode, it is necessary to verify whether Rossiter and/or centrifugal modes can be related to the bypass transition observed in Crouch *et al.* (2022) where Beguet *et al.* (2017) data was used. Therefore, the present study consists of a numerical and theoretical study of the boundary layer stability containing a cavity, with gaps similar to those covered by Crouch *et al.* (2022). Table 1 summarizes the key simulation parameters employed, such as the cavity geometry, Reynolds, and Mach numbers. The selected gaps are in the vicinity of the horizontal bounds from Fig. 1, with $L/\delta^*(w/\delta^*)$ between 40 and 50. Case 1 corresponds to a cavity in the imminence of the bypass transition (open red marker), whereas case 2 simulates a cavity that causes bypass transition (filled red marker).

Table 1. Input parameters for DNS simulations.

Case	D/δ^*	L/δ^*	Re_{δ^*}	M_∞
1	1.7	42.7	1416	0.053
2	1.8	45.3	1467	0.060

2. Methodology

Direct numerical simulation (DNS) for compressible Navier Stokes equations was used to perform the simulation, with an in-house code developed by the aeroacoustics, transition and turbulence group (GATT) of the aeronautical engineering department of the São Carlos engineering school of the University of São Paulo (EESC-USP), better detailed and validated in Mathias *et al.* (2016) and Mathias and Medeiros (2017). In this code the approaches and considerations were:

- Structured mesh (2D or 3D) Mesh stretching to concentrate nodes in the regions of interest;
- Compressible flow;
- 4-order Runge-Kutta approximation for time advance;
- Structured Cartesian mesh with stretching to concentrate nodes in regions of interest;
- sixth-order spectral-like finite differences spatial derivatives;
- Buffer-zones at the open boundaries;
- 10th order spatial anti-aliasing filter;
- Temporal low-pass filter (SFD) to allow reaching a base-flow even ate unstable conditions.

After the flow simulation, a simulation time was defined for the flow state is in the limit cycle regime. From this state the SFD was used to identify and damp the most unstable mode, and by the method presented in Åkervik method this process was repeated so that the highest frequency present in the flow was considered residual. The result of this process is a baseflow, a flow in which all its initial frequencies have been damped, this process is essential in unsteady cases, because it is impossible to achieve a time invariant flow without the use of a relaxation technique. the method of Åkervik *et al.* (2006) was used for this damping.

For the analysis of linear stability we use the baseflow found, when the case is unstable, or the flow itself when it is stable. In a 2D linear stability analises the unstable modes are compared to the Rossiter modes, and in a 3D linear stability analises the instability effects that may occur are related to the centrifugal modes.

3. Results

3.1 DNS

Concerning first run, Fig. 2a shows the maximum absolute variation of the flow variables as a function of non-dimensional time tU/δ^*. These signals indicate that the simulation converged to a time-invariant Navier-Stokes solution for the first cavity, Fig. 2a, without the employ of the SFD, while for the second cavity, these signals not converged, Fig. 2b, therefore it was necessary to apply SFD subsquently.

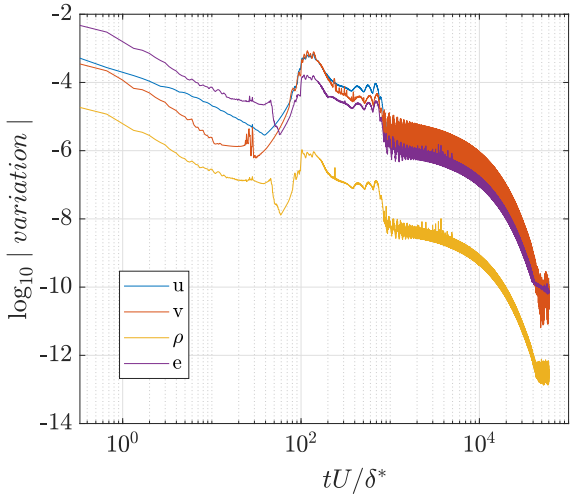

(a) Maximum absolute variation of the flow variables in the first cavity.

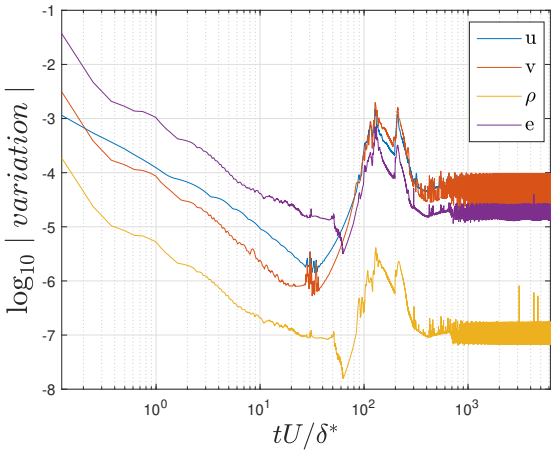

(b) Maximum absolute variation of the flow variables in the second cavity.

Figure 2. Maximum absolute variation of the flow variables.

Figure 3a, where the contours represent the velocity variable in the direction normal to the wall, at Fig. 3a, shows that the flow, in the region of the cavity, has the presence of vortices only inside the cavity, outside the cavity it is no longer possible to verify the existence of vortices shedding. while, Fig. 3b shows a flow in limit cycle regime, in this flow there are, inside the cavity, variations in velocity perpendicular to the wall, this oscillatory motion occurs due to the emission of vortices by the cavity. These are convected, collide at the first corner of the cavity and persist on the boundary layer downstream of the cavity for at least two cavity lengths. This mechanism resembles the mechanism described by Mathias and Medeiros (2018).

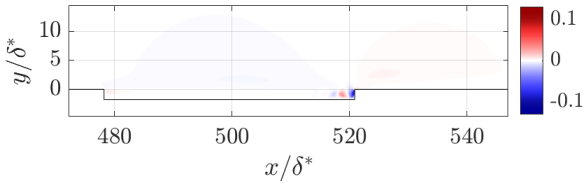

(a) Speed contours normal to the wall referring to run 1.

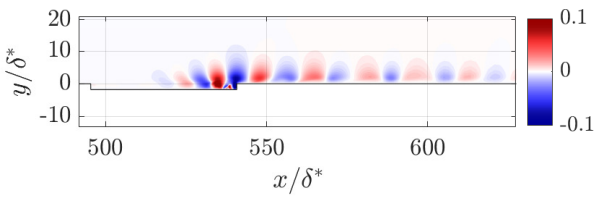

(b) Velocity perpendicular to the wall, of run 2 in cyclic regime.

Figure 3. Speed contours normal to the wall.

3.2 Baseflow

Because the flow at second cavity did not stabilize spontaneously, it was necessary to apply the SFD. After applying the filter to the entire domain, the flow was artificially stabilized, as shown in fig. 4, the simulation variables converged to a magnitude of e-11, which proves a stationary flow.

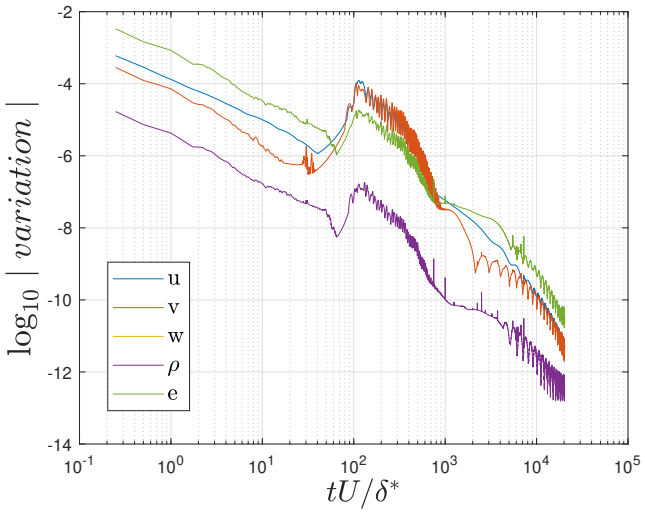

Figure 4. SFD damping of the simulation variables in run 2.

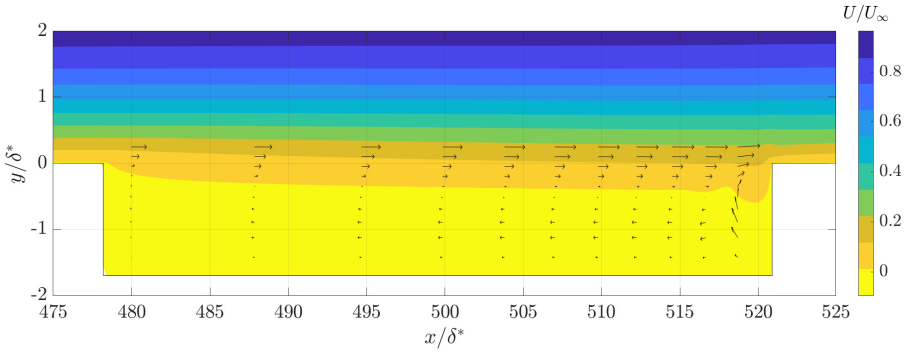

Figure 5. Velocity contours parallel to the flat plate and velocity vectors at mesh points in case 1, without the use of SFD.

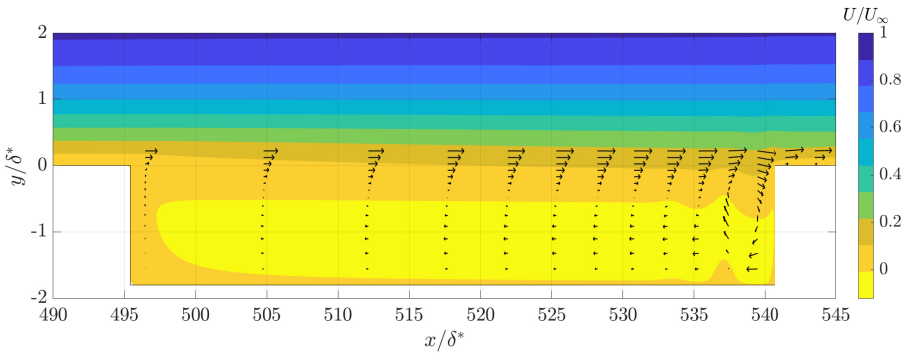

Figure 6. Velocity contours parallel to the flat plate and velocity vectors at mesh points in case 2, using SFD.

3.3 2D Stability analysis

In addition, a 2D linear stability theory (LST) stability analysis was performed to the base flows found, in order to obtain the eigenfunctions and eigenvalues inherent to the parameters in question. Figure 7a shows the eigenvalues of the modes found. The convergence of the values of the moduli can be checked in the table such that it shows the value of

the most unstable mode in the last iteration and at iteration number 250 in krilov space. Other convergence values had a similar order of magnitude to those presented in the Tab. 2

Table 2. Real value of the least stable eigenvalue at different iterations in LST 2D for the first cavity.

iteration	**Real (eigenvalue)** $\cdot 10^{-4}$
150	7.051822
200	7.051837

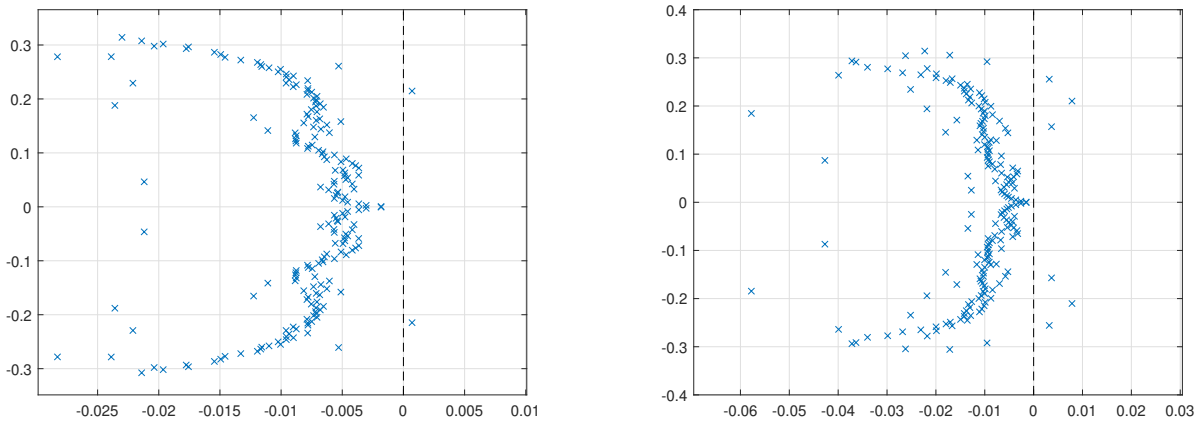

(a) Eigenvalues of the 2D modes of the first run. (b) Eigenvalues of the 2D modes of the second run.

Figure 7. Eigenvalues in 2D stabiliy analysis.

Table 3. Unstable eigenvalues value of run 1.

Modes
$0.0007051 \pm i0.214689$

Table 4. Unstable eigenvalues value of run 2.

Modes
$0.0078489 \pm i0.2102252$
$0.0036620 \pm i0.1570064$
$0.0031998 \pm i0.2557079$

Even though case one was initially stable, by means of LST analysis this run is shown to have unstable modes. The frequency of the unstable mode corresponds to 0.214689, when converted to the appropriate units by Eq. 1.

$$\frac{fL}{U} = \frac{0.214689L}{2\pi\delta^*} = 1.459 \tag{1}$$

For the second case, the frequencies of the obtained modes, when non-dimensionalized in the same way, are as follows in the Tab. 5.

When these frequencies are compared to the Rossiter's frequencies by the equation that calculates the possible frequencies of a rossiter from BLOCK

$$\frac{fL}{U} = \frac{m}{\frac{1}{K} + M(1 + \frac{0.514}{L/D})} \tag{2}$$

where f, L, D and U are frequency, length of cavity, depth and normal velocity to the wall respectively, and m, K and M are rossiter mode numbers, a constant and Mach number respectively, The value adopted for K is the value cited by Crouch *et al.* (2022) where it assumed the value of 0.57. The values of Rossiter's frequencies obtained for the second cavity differ only in the second digit after the decimal point, so the comparison with the non-dimensionalized frequencies

Table 5. Admensionalized frequencies of run 2.

Frequency
1.5156
1.1319
1.8435

of the modes present in the second run can be compared with the values in Tab. 6.. Then the value of m for the first cavity, that results in the closest frequency to the present mode frequency is 3, such that $FL/U = 1.6589$ as can be seen in the Tab. 6. it is possible For the second cavity, can the frequencies correlate with the Rossiter frequencies, being the one with the lower frequency compatible with a Rossiter 2 and the other two modes compatible with Rossiter 3,

Table 6. Rossiter mode numbers and their possible estimated frequencies from Block (1976) in run 1.

m	**fL/U**
1	0.5530
2	1.1059
3	1.6589
4	2.2118

In general, the mode of a Rossiter can be determined by the number of times a pair of velocity reversals occurs perpendicular to the wall in an eigenfunction plot. In Fig. 8, the eigenfunctions of the unstable modes in case 2 are shown, and it can be observed that the reversal of velocity direction within the cavity occurs twice in Fig. 8b and three times in Fig. 8a and Fig. 8c, as expected for Rossiter modes 2 and 3, respectively. The same behavior could be observed in the eigenfunction of the unstable mode in case 1, which characterized a Rossiter mode 3

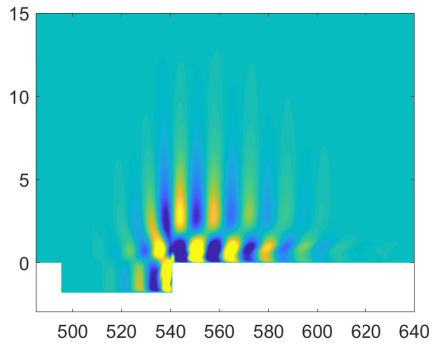

(a) Eigenfunction of the most unstable mode, run 2.

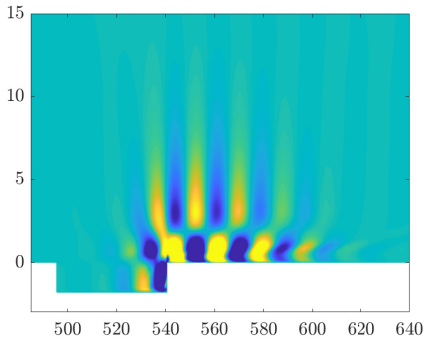

(b) Eigenfunction of the second most unstable mode, run 2

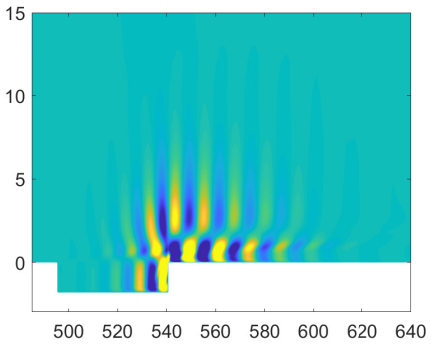

(c) Eigenfunction of the third most unstable mode, run 2.

Figure 8. Eigenfunctions of the unstable modes present in run 2.

3.4 3D Stability analysis

Finally, a 3D LST analysis depicts the evolution of the most unstable three-dimensional modes while varying the beta variable to achieve the desired lambda values, so that

$$\frac{\lambda}{D} = \frac{2\pi}{\beta} \tag{3}$$

where λ is the wavelength of the disturbance, and β is the wavenumber.

Initially, beta values were chosen so that the value of λ/D is close to the unstable region demonstrated in the cases of Brès and Colonius (2008). The first λ/D value used was 1.8. For cavity 1, unstable centrifugal modes were found in the range of λ/D between 1.4 and 6.2, with each group of markers in Fig. 9a corresponding to the eigenvalues of the modes induced by a specific λ/D. In Fig. 10a, the real value of the most unstable eigenvalue is shown as a function of λ/D. The same scheme was organized for cavity 2, where unstable centrifugal modes were observed in a λ/D range of 6.2 to 8.0. Fig. 9b indicates the eigenvalues found when $\lambda/D = 7.2$ is applied, and Fig. 10b shows the values of the real part of the most unstable eigenvalues as a function of λ/D.

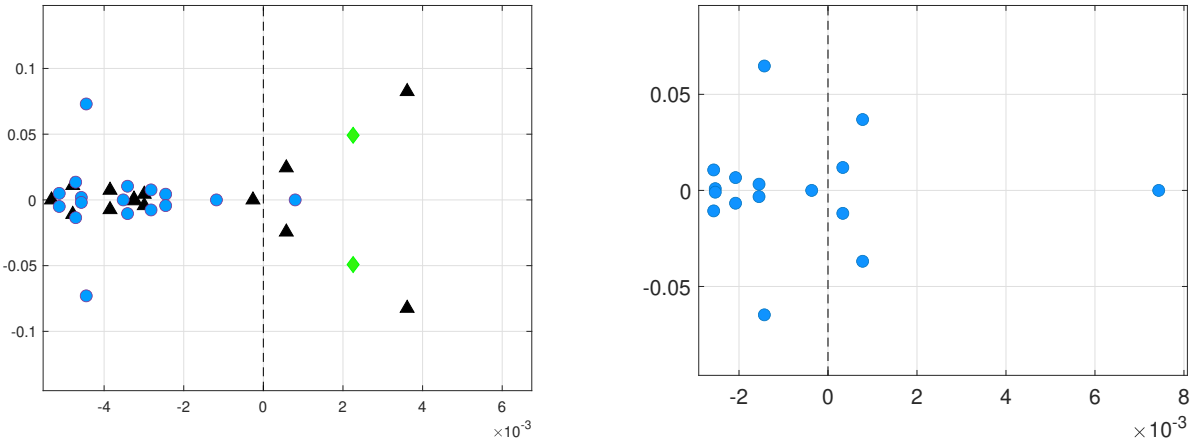

(a) Eigenvalues found in case 1.

(b) Eigenvalues found in case 2.

Figure 9. Eigenvalues found from a 3D stability analysis using LST.

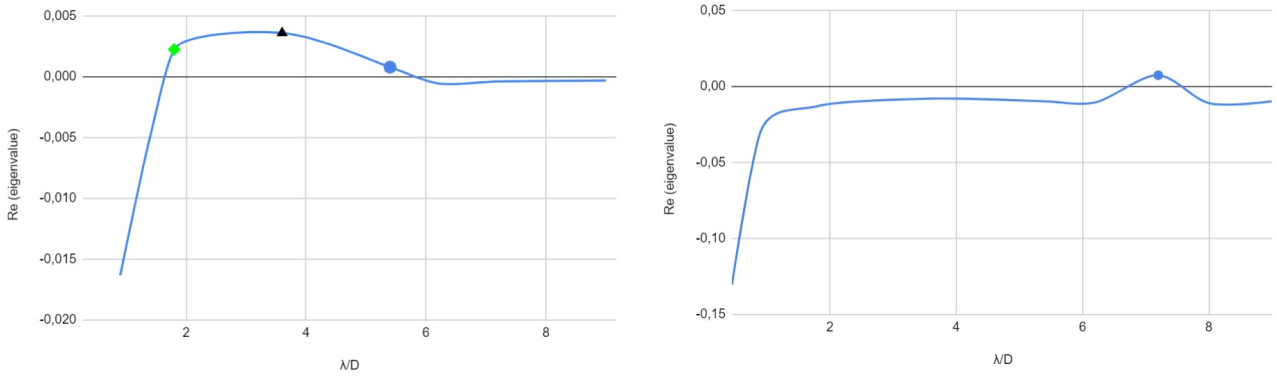

(a) Real part of the most unstable eigenvalue as a function of λ/D, in run 1.

(b) Real part of the most unstable eigenvalue as a function of λ/D, in run 2.

Figure 10. Real part of the most unstable eigenvalue as a function of λ/D.

The eigenfunctions of the centrifugal modes found help determine the type of centrifugal mode. Therefore, the figures, Fig.11a, Fig.11b, Fig.11c, correspond to the eigenfunctions of the most unstable modes that appeared at each λ/D value that exhibited instability in the first cavity. Fig.12 illustrates the eigenfunction of the most unstable mode related to the 3D stability analysis of the second cavity.

The eigenfunctions found can be used for comparison with the linear stability analysis of other cavities, identifying similarities between them and the type of centrifugal mode.

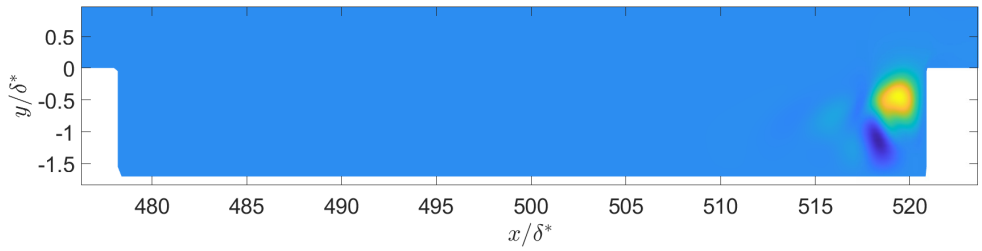

(a) Eigenfunction of the most unstable mode at $\lambda/D = 1.8$, in case 1.

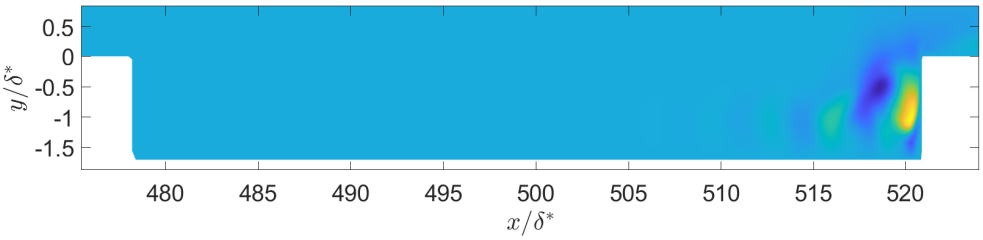

(b) Eigenfunction of the most unstable mode at $\lambda/D = 3.6$, in case 1.

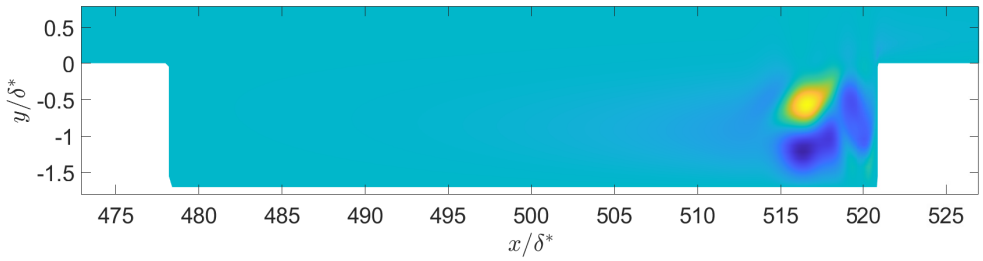

(c) Eigenfunction of the most unstable mode at $\lambda/D = 5.4$, in case 1.

Figure 11. Eigenfunctions of the unstable 3D modes present in case 1.

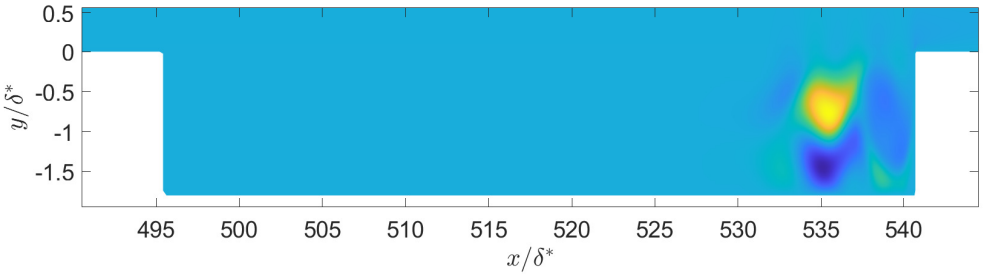

Figure 12. Eigenfunction of the unstable 3D mode present in case 2.

4. ACKNOWLEDGEMENTS

The authors would like to thank the Institutional Scientific Initiation Scholarship Program (PIBIC) for grants 2022/2633, the Coordenação de Aperfeiçoamento de Pessoal de Nível Superior (CAPES)- Programa de Excelência Acadêmica (PROEX) - Brasil for Financial Support. M.A.F.M. is sponsored by CNPq/Brazil (grant no.307956/2019-9), sponsored by FAPESP (grant no. 2019/15336-7) and the US Air Force Office of Scientific Research (AFOSR) for grant FA9550-18-1-0112, managed by Dr. Geoff Andersen from SOARD. and all the researchers in the Aeroacoustics, Transition and Turbulence Group (GATT) of the aeronautical engineering department of the São Carlos engineering school of the University of São Paulo (EESC-USP).

5. REFERENCES

Åkervik, E., Brandt, L., Henningson, D.S., Hœpffner, J., Marxen, O. and Schlatter, P., 2006. "Steady solutions of the Navier-Stokes equations by selective frequency damping". *Physics of Fluids*, Vol. 18, No. 6, p. 68102. ISSN 10706631. doi:10.1063/1.2211705. URL `http://scitation.aip.org/content/aip/journal/pof2/18/6/10.1063/1.2211705`.

Beguet, S., Perraud, J., Forte, M. and Brazier, J.P., 2017. "Modeling of Transverse Gaps Effects on Boundary-Layer Transition". *Journal of Aircraft*, Vol. 54, No. 2, pp. 794–801. ISSN 0021-8669. doi:10.2514/1.C033647. URL https://arc.aiaa.org/doi/10.2514/1.C033647.

Block, P.J.W., 1976. "Noise response of cavities of varying dimensions at subsonic speeds". *Technical report*, Vol. NASA TN D-.

Brès, G.A. and Colonius, T., 2008. "Three-dimensional instabilities in compressible flow over open cavities". *Journal of Fluid Mechanics*, Vol. 599, pp. 309–339. ISSN 0022-1120. doi:10.1017/S0022112007009925. URL http://www.journals.cambridge.org/abstract$_S$0022112007009925.

Crouch, J.D., Kosorygin, V.S., Sutanto, M.I. and Miller, G.D., 2022. "Characterizing surface-gap effects on boundary-layer transition dominated by Tollmien-Schlichting instability". *Flow*, Vol. 2. ISSN 26334259. doi:10.1017/flo.2022.1.

de Vicente, J., Basley, J., Meseguer-Garrido, F., Soria, J. and Theofilis, V., 2014. "Three-dimensional instabilities over a rectangular open cavity: from linear stability analysis to experimentation". *Journal of Fluid Mechanics*, Vol. 748, pp. 189–220. ISSN 0022-1120. doi:10.1017/jfm.2014.126. URL http://www.journals.cambridge.org/abstract$_S$0022112014001268.

Mathias, M. and Medeiros, M.F., 2018. "The Influence of the Boundary Layer Thickness on the Stability of the Rossiter Modes of a Compressible Rectangular Cavity". In *2018 Fluid Dynamics Conference*. American Institute of Aeronautics and Astronautics, Reston, Virginia. ISBN 978-1-62410-553-1. doi:10.2514/6.2018-3386. URL https://arc.aiaa.org/doi/10.2514/6.2018-3386.

Mathias, M.S., Martinez, A.G. and Medeiros, M.A.F., 2016. "Direct numerical simulation of a flow and matrix-free analysis of its instabilities over an open cavity". In *Proceedings of the 10th ABCM Spring School on Transition and Turbulence*. ABCM, São José dos Campos, SP, Brazil.

Mathias, M.S. and Medeiros, M.A.F., 2017. "Direct numerical simulation of a compressible flow and matrix-free analysis of its instabilities over an open cavity". *Journal of Aerospace Technology and Management (Accepted for publication)*.

Mathias, M.S. and Medeiros, M.A., 2021. "The effect of incoming boundary layer thickness and Mach number on linear and nonlinear Rossiter modes in open cavity flows". *Theoretical and Computational Fluid Dynamics*, Vol. 35, No. 4, pp. 495–513. ISSN 14322250. doi:10.1007/s00162-021-00570-2. URL https://doi.org/10.1007/s00162-021-00570-2.

Meseguer-Garrido, F., de Vicente, J., Valero, E. and Theofilis, V., 2014. "On linear instability mechanisms in incompressible open cavity flow". *Journal of Fluid Mechanics*, Vol. 752, pp. 219–236. ISSN 0022-1120. doi:10.1017/jfm.2014.253. URL http://www.journals.cambridge.org/abstract$_S$0022112014002535.

Rossiter, J.E., 1964. "Wind-tunnel Experiments on the Flow Over Rectangular Cavities at Subsonic and Transonic Speeds". Report, Ministry of Aviation; Royal Aircraft Establishment; RAE Farnborough.

Rowley, C.W., Colonius, T. and Basu, A.J., 2002. "On self-sustained oscillations in two-dimensional compressible flow over rectangular cavities". *Journal of Fluid Mechanics*, Vol. 455, pp. 315–346. ISSN 0022-1120. doi:10.1017/S0022112001007534.

Sun, Y., Taira, K., Cattafesta, L.N. and Ukeiley, L.S., 2017. "Biglobal instabilities of compressible open-cavity flows". *Journal of Fluid Mechanics*, Vol. 826, pp. 270–301. ISSN 0022-1120. doi:10.1017/jfm.2017.416. URL https://www.cambridge.org/core/product/identifier/S0022112017004165/type/journal$_a$$rticle$.

Yamouni, S., Sipp, D. and Jacquin, L., 2013. "Interaction between feedback aeroacoustic and acoustic resonance mechanisms in a cavity flow: a global stability analysis". *Journal of Fluid Mechanics*, Vol. 717, pp. 134–165. ISSN 1469-7645.

6. RESPONSIBILITY NOTICE

The authors are solely responsible for the printed material included in this paper.